SAND2020-10836C

Transient Thermal Performance of High-Temperature Particle Storage Bins

Kaden Plewe,[1, a)] Jeremy N. Sment,[2] Mario J. Martinez,[3] Clifford K. Ho,[2] and Dongmei Chen[1]

[1] *The University of Texas at Austin Department of Mechanical Engineering, 204 E. Dean Keeton Street, Stop C2200, Austin, TX 78712-1591, USA*
[2] *Sandia National Laboratories, P.O. Box 5800, MS-1127, Albuquerque, NM 87185-1127, USA*

[a)]Corresponding author: plewe.kaden@utexas.edu

Abstract. The design, modeling, and integration of high-temperature particle storage bins is a critical component of Gen. 3 concentrated solar power (CSP). Particle storage bins control the temperature and flow rates throughout the particle circulatory system, so having a fundamental understanding of their transient thermal behavior is highly advantageous for the design and multi-level control of future CSP systems. This paper provides contributions to this understanding by presenting a semi-analytic method for modeling the transient thermal behavior of bulk particle bins. The model is verified with experiments and a baseline CFD model and then used to make conclusions about the dominant heat transfer modes in bulk particle bins and the general transient thermal performance of related systems.

INTRODUCTION

Advancements in particle-based concentrated solar technology are demonstrating improvements in performance and levelized cost of electricity (LCOE) for the next generation of concentrated solar power (CSP). In particular, the Generation 3 Particle Pilot Plant (G3P3), a pilot-scale demonstration project that began in 2018, is being designed to test an integrated thermal CSP system with a thermal duty of 1 MW and 6 MWh of thermal storage. The commercial-scale version of this particle-based CSP system is expected to yield an LCOE below 0.06 $/kWh$_e$ [1].

One novel aspect of the G3P3 system that can drive down the LCOE is its thermal storage system [2]. After particles are heated to ~800 °C in the solar receiver, they are stored in a hot storage bin before passing through a particle-to-working-fluid heat exchanger, which is the point-of-coupling with a supercritical CO_2 Brayton Cycle, and then into a cold storage bin at ~600 °C [1], [3]. Thus, it is established that the hot-particle storage bin is a critical regulatory mechanism for 1) the on-demand thermal duty of the particle circulatory system and 2) the active participation of the G3P3 system in grid-wide dispatching operations for power transmission and distribution.

The dynamics and thermal behavior related to the operation of particle storage bins is not necessarily trivial. A lumped-model approach to capturing the salient physics is not sufficient for the integrated application of these bins in complex systems, which motivates the targeted thermal-dynamic modeling and experimental efforts presented in this paper. The literature is quite rich in the dynamic characterization of bulk particle bins, as the kinematic and stress-related implications are historically applicable to agriculture, mining, manufacturing and the like. Many of the theoretical and experimental developments in this field began with the early work of Andrew Jenike [4], where he considers the continuous flow of rigid-plastic solids. Perhaps one of the most cited of Jenike's results is his derived analytical equation for characterizing the conditions under which the flow regime in a bulk-particle bin transitions from mass-flow to funnel-flow, with one of the most influential parameters being the hopper half-angle, $\alpha°$ (see **FIGURE 1**). This and many other works (e.g. [5]–[11]) have established a solid platform for the study and design of

Sandia National Laboratories is a multimission laboratory managed and operated by National Technology & Engineering Solutions of Sandia, LLC, a wholly owned subsidiary of Honeywell International Inc., for the U.S. Department of Energy's National Nuclear Security Administration under contract DE-NA0003525.

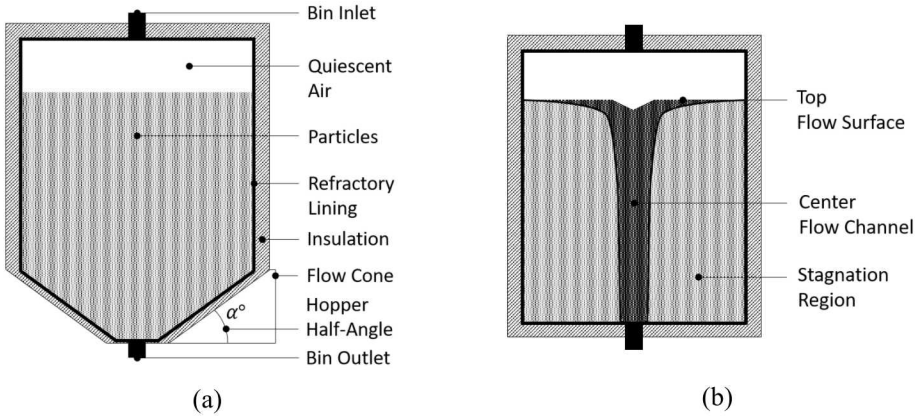

FIGURE 1. Particle storage bin nomenclature general to all bin geometries (a) and unique to funnel flow regimes (b)

granular solid storage bins in situations where the dynamic performance is generally isolated from thermal considerations. However, there is a considerable gap in the literature with regard to thermal-dynamic coupling.

High-temperature particle bins have been given a spotlight for their long-term thermal storage capacity in renewable energy systems [12], [13], so it is no question that the thermal analysis of such systems will be a high-demand topic in the coming years. As of now, there is no comprehensive understanding of the thermal transient behavior of bulk solids in storage bins. Efforts in this realm have been quite sparse in scope, tending to focus generally on the diffusive properties of bulk solids or on the lumped behavior (i.e. overall thermal performance) of particle storage bins. The interspatial heat transfer characteristics in bulk particles has been the focus of a number of interesting foundational works [14], [15] and it is generally agreed upon that a bulk thermal conductivity model is appropriate in the application of particle thermal storage bins [16]–[18].

The consideration of thermal performance in high-temperature particle storage bins has been addressed generically in terms of the thermal resistance separating the hot particles from the surroundings. Designing to this thermal performance criterion consists of minimizing the bin surface area and maximizing the effectiveness of bin insulation within a given design space and has been studied extensively for the G3P3 system [3], [16] and elsewhere [19]. In this paper, we take a new step in exploring the more detailed thermal characterization of high-temperature particle storage bins. It is, perhaps, analogous to that which was taken some 80 years ago with regard to the dynamic characterization of the same system, in that we are now attempting to understand the fundamental thermal interactions in the particle domain. In doing so, we hope to expand the definition of thermal performance to encompass aspects of predictability, controllability, and reliability; as these are, of course, critical in a highly integrated thermal storage system.

Contributions

The work presented in this paper is the beginning of what will be a more comprehensive characterization of the heat transfer modes that influence the thermal performance of high temperature particle storage bins that will be found in future work. With that said, it is the authors' intention herein to provide contributions to this progression with the following.

1) The introduction of a new method for modeling the momentum and energy movement within high-temperature particle storage bins is provided.
2) The dominant heat transfer modes in high-temperature particle storage bins are explicitly identified.
3) A comparison of the thermal performance for mass-flow versus funnel-flow regimes is provided.
4) An experimental and model baseline verification is provided for the transient outlet temperature in particle storage bins.
5) A comprehensive definition for the thermal performance of high-temperature particle storage bins in a CSP application is suggested.

PARTICLE STORAGE BIN MODEL

We start by identifying a set of criteria for particle storage thermal models applied to the G3P3 or other CSP systems. The model should be 1) computationally efficient to support generic usage and real-time implementation, 2) deterministic and scalable to accommodate design and operational efforts and 3) control oriented to support advanced controls for the integration of the thermal storage tank with the broader CSP system. The first criterion eliminates the option of taking a full CFD approach, since sufficiently capturing the momentum and energy interactions requires a highly refined spatial and temporal discretization. This is, however, a desirable approach where resources permit and has been implemented in the form of a numerical level-set model in previous G3P3 works [16], [20]. The second criterion nullifies data-driven methods. While the ever-growing field of data-driven modeling techniques may be able to provide high-accuracy predictions, it would provide no basis for fundamental understanding and is therefore removed from consideration. Finally, a fully analytical approach is not practical with established theory and would otherwise require excessive simplification. With this brief survey, we establish the justification for the modeling approach presented here.

What is proposed here is a semi-analytic model, where a heat kernel for a partial domain is derived using standard analytical methods and coupled to the remaining particle domains with a set of transfer functions. These transfer functions can be either analytically or numerically derived. The particle domain separation follows from established experimental and theoretical work on particle kinematics, as cited previously. For the mass flow regime, we separate the particle domain according to **FIGURE 1(a)** into 1) a cylindrical region and 2) a flow cone region. For the funnel flow regime, we separate the particle domain according to **FIGURE 1(b)** into 1) a stagnant region, 2) a top flow surface and 3) a center flow channel. With this partitioning, the heat transfer modes and boundary conditions shown in **FIGURE 2** are identified and made central to the development of the model. Note that **FIGURE 2** indicates a boundary condition of the fifth kind (Jaeger) for the storage bin wall, which functions as a thin-film capacitor with a prescribed exterior heat transfer coefficient, h_∞. While this wall-capacitance is evidently neglected in this work, it will be a critical component in future work, where the model is used to represent the full cyclic behavior of the thermal storage system. In a cyclic situation, the thermal capacitance of the refractory lining and bin insulation should not be neglected. The moving-boundary component that is inherent to the charge-discharge process of the particle storage bin is accounted for numerically with a temporal discretization, and is emphasized throughout this paper using a superscript, $[\cdot]^k$, on terms that are re-evaluated at each time step.

The framework set forth here for modeling the transient thermal behavior of particle domains is based foundationally on the theory of Green's functions for mapping an energy impulse to an associated thermal response. In particular, our modelling efforts seek to set a platform for mapping the thermal-dynamic behavior of flowing particle regions and transient boundaries to an associated heat kernel. The problem, then, is reduced to solving for each partitioned particle domain individually with the assumption of known boundary conditions and then finding a transfer function to couple each region to reformulate the original domain. In determining the transfer functions, care must be taken to ensure 1) that the problem is well-defined and 2) that first-principles are satisfied. The implications of this and other more detailed aspects of the model will be addressed in future publications.

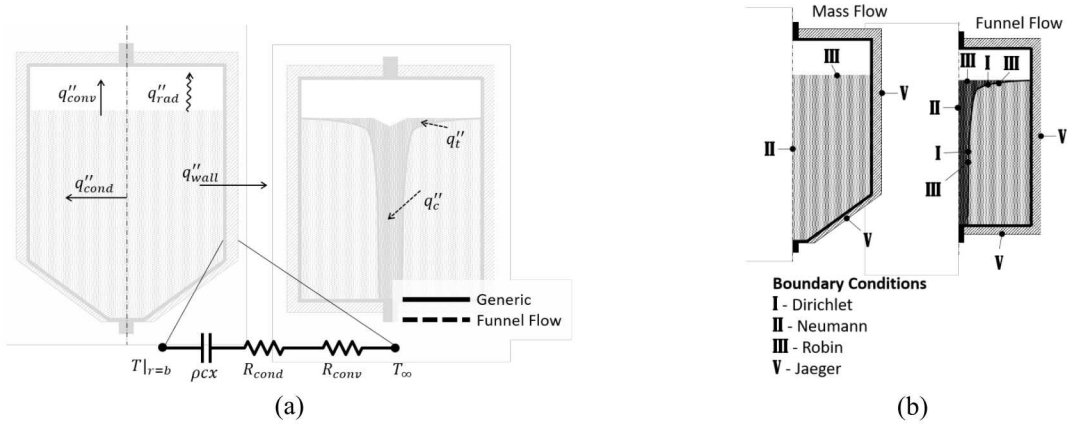

FIGURE 2. Heat transfer modes considered (a) and boundary conditions (b)

Heat Kernel Derivation

The heat kernel is derived as a traditional Green's function for heat conduction [21]. This is valid only for a stagnant body. Hence, the funnel flow heat kernel is derived for the stagnant particle region and the mass flow heat kernel is derived for the cylindrical particle region. Note that the mass flow particles in the cylindrical region are assumed to shift uniformly as a bulk body, which is the basis for their treatment as a stagnant body with respect to a moving reference frame. The method of Green's functions has traditionally been used to allow for solutions to be derived for linear conduction problems that have transient and spatially inhomogeneous boundaries and/or generation terms. In relation to the work herein, there has been some exciting recent development in the application of Green's functions for deriving semi-analytic solutions that alleviate the mathematical complexity involved in computing integrals that arise in related formulae [22], [23]. More traditional usage of the Green's function method is still highly relevant as well, such as in [24] and [25].

Although it is certainly not the only way, the Green's function is derived here by solving the homogeneous counterpart of the overall conduction problem and then applying a variable transformation. For a comprehensive understanding of this method, the interested reader is directed to [21] and [27]. The homogeneous counterparts that are used to solve for the funnel flow heat kernel, $G_{ff}^{k}(r,z,t|r',z',\tau)$, and the mass flow heat kernel, $G_{mf}^{k}(r,z,t|r',z',\tau)$, are outlined in **TABLE 1**. The notation used for the Green's function can be interpreted as follows: the function $G(r,z,t|r',z',\tau)$ computes the thermal response at location (r,z) and time t due to an instantaneous impulse released at location (r',z') and time τ.

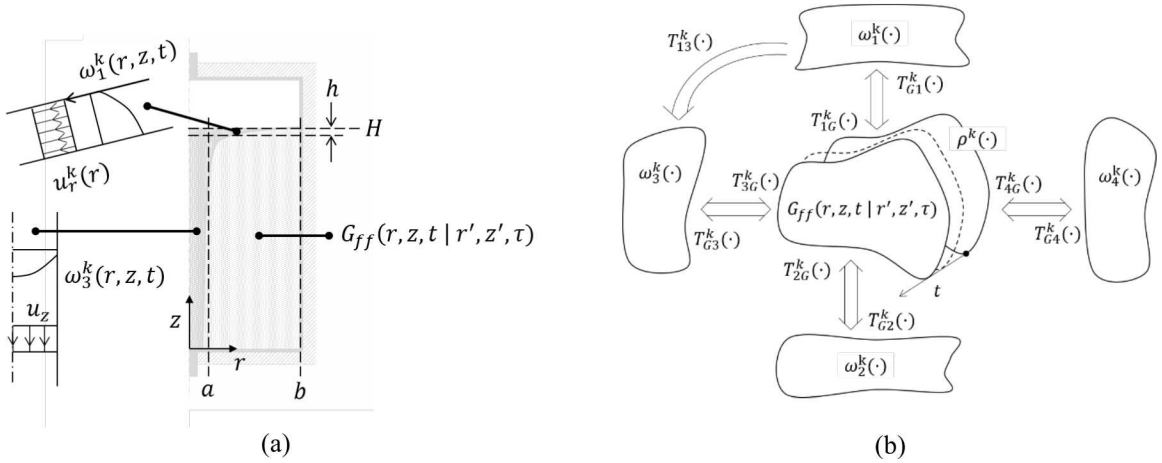

FIGURE 3. Funnel flow model domain separation (a) and general framework used for thermal domain coupling (b)

TABLE 1. Governing equation, boundary conditions, and general solution for derived heat kernels. Initial conditions are known and arbitrary.

	Governing Eq.	r-boundaries	z-boundaries	Solution	Notes
$G_{ff}^{k}(r,z,t\|r',z',\tau)$	$\frac{1}{\alpha}\frac{\partial G_{ff}^{k}}{\partial t} = \nabla^2 G_{ff}^{k}$	$-\left.\frac{\partial G_{ff}^{k}}{\partial r}\right\|_{r=a} + Bi_3 G_{ff}^{k}\|_{r=a} = 0$ $\left.\frac{\partial G_{ff}^{k}}{\partial r}\right\|_{r=b} + Bi_4 G_{ff}^{k}\|_{r=b} = 0$	$-\left.\frac{\partial G_{ff}^{k}}{\partial z}\right\|_{z=0} + Bi_2 G_{ff}^{k}\|_{z=0} = 0$ $\left.\frac{\partial G_{ff}^{k}}{\partial z}\right\|_{z=H-h} + Bi_1 G_{ff}^{k}\|_{z=H-h} = 0$	[26]	*
$G_{mf}^{k}(r,z,t\|r',z',\tau)$	$\frac{1}{\alpha}\frac{\partial G_{mf}^{k}}{\partial t} = \nabla^2 G_{mf}^{k}$	$\left.\frac{\partial G_{mf}^{k}}{\partial r}\right\|_{r=0} = 0$ $\left.\frac{\partial G_{mf}^{k}}{\partial r}\right\|_{r=b} + Bi_4 G_{mf}^{k}\|_{r=b} = 0$	$\left.\frac{\partial G_{mf}^{k}}{\partial z}\right\|_{z=0} = 0$ $\left.\frac{\partial G_{mf}^{k}}{\partial z}\right\|_{z=H} + Bi_5 G_{mf}^{k}\|_{z=H} = 0$	[27]	*

* Bi_n is the Biot number at the corresponding boundary w.r.t. an arbitrary scaling dimension.

Thermal Domain Coupling

The three partitioned domains that make up the funnel flow regime are shown in **FIGURE 3(a)**. For both of the flowing regions, the dynamic solutions are simplified with a plug-flow assumption. While this isn't necessarily indicative of the true momentum flux through the domain, it appears to be sufficient for the purpose of capturing the advective heat transfer through these regions. The energy equation in both of these domains can be solved with the corresponding kinematic profiles, as is outlined with the remaining boundary conditions in **TABLE 2**.

The transfer functions that allow us to couple the partitioned regions will not be discussed in detail here, although their attainment is rather straight forward. However, their application is demonstrated in **FIGURE 3(b)**, where the framework for the full funnel flow model is drawn. This framework is realized mathematically through the well established Green's function formula, the derivation of which can be found in [27]. The funnel flow Green's formula is

$$\begin{aligned}\theta_{ff}^{k}(r,z,t) = &\int_{0}^{H-h}\int_{a}^{b} G_{ff}^{k}(r,z,t|r',z',\tau)|_{\tau=0}\rho^{k}(r',z')\ dr'dz' \\ &+\int_{\tau=0}^{t}\int_{a}^{b} G_{ff}^{k}(r,z,t|r',z',\tau)|_{z'=H-h}T_{1G}^{k}(r',\tau)\ dr'd\tau \\ &+\int_{\tau=0}^{t}\int_{0}^{H-h} G_{ff}^{k}(r,z,t|r',z',\tau)|_{r'=a}T_{3G}^{k}(z',\tau)\ dz'd\tau\ ,\end{aligned} \tag{1}$$

where $\theta_{ff}^{k}(r,z,t)$ is the transient temperature distribution in the stagnant region, $\rho^{k}(r',z')$ is the initial condition and $T_{1G}^{k}(r',\tau)$ and $T_{3G}^{k}(z',\tau)$ are the boundary-to-kernel transfer functions for the top flow surface and center flow channel, respectively. Note that the remaining boundaries, ω_2^k and ω_4^k, are not explicitly included in Eq. 1 because they are intrinsic to the heat kernel. Similarly, the mass flow Green's formula is

$$\theta_{mf}^{k}(r,z,t) = \int_{0}^{H}\int_{0}^{b} G_{mf}^{k}(r,z,t|r',z',\tau)|_{\tau=0}\zeta^{k}(r',z')\ dr'dz'\ , \tag{2}$$

where $\zeta^{k}(r',z')$ is the initial condition for the cylindrical region. Here, all boundaries for the heat kernel are intrinsic to its derivation. The remaining temperature distribution in the flow cone is solved for according to the information listed in **TABLE 3**. In the results presented in this paper, the temperature distribution in the flow cone is one-dimensional. This is purely for simplification purposes and was justified in this application because we are primarily concerned with the total heat loss attributed to the flow cone region. This simplification is conservative and also preserves monotonicity.

TABLE 2. Governing equation, boundary conditions, and general solution to funnel flow heat kernel boundary couplings. Initial conditions are known and arbitrary.

	Governing Eq.	r-boundaries	z-boundaries	Solution	Notes
$\omega_1^k(r,z,t)$	$\frac{1}{\alpha}\frac{D\omega_1^k}{Dt} = \nabla^2\omega_1^k$	$\left.\frac{\partial\omega_1^k}{\partial r}\right\|_{r=a} = 0$ $\omega_1^k\|_{r=b} = cte$	$\omega_1^k\|_{z=0} = T_{G1}^k(r)$ $\left.\frac{\partial\omega_1^k}{\partial z}\right\|_{z=h} + H_1\omega_1^k\|_{z=h} = cte$	$e^{A_1^k t}\omega_1^k\|_{t_0}$	*, †, ▲
ω_2^k	–	–	–	T_∞	**
$\omega_3^k(r,z,t)$	$\frac{1}{\alpha}\frac{D\omega_3^k}{Dt} = \nabla^2\omega_3^k$	$\left.\frac{\partial\omega_3^k}{\partial r}\right\|_{r=0} = 0$ $\omega_3^k\|_{r=a} = T_{G3}^k(z)$	$\omega_3^k\|_{z=H} = cte$ $\left.\frac{\partial\omega_3^k}{\partial z}\right\|_{z=0} = 0$	$e^{A_3^k t}\omega_3^k\|_{t_0}$	*, †
ω_4^k	–	–	–	T_∞	**

* A_1^k and A_3^k are state matrices derived from a spatial discretization of the domain, updated at every time-step, k.

† 'cte' refers to a constant condition over time-step, k.

▲ H_1 is the ratio of the boundary heat transfer coefficient to the bulk particle thermal conductivity.

** Homogeneous simplification from Jaeger boundary condition shown in **FIGURE 2**.

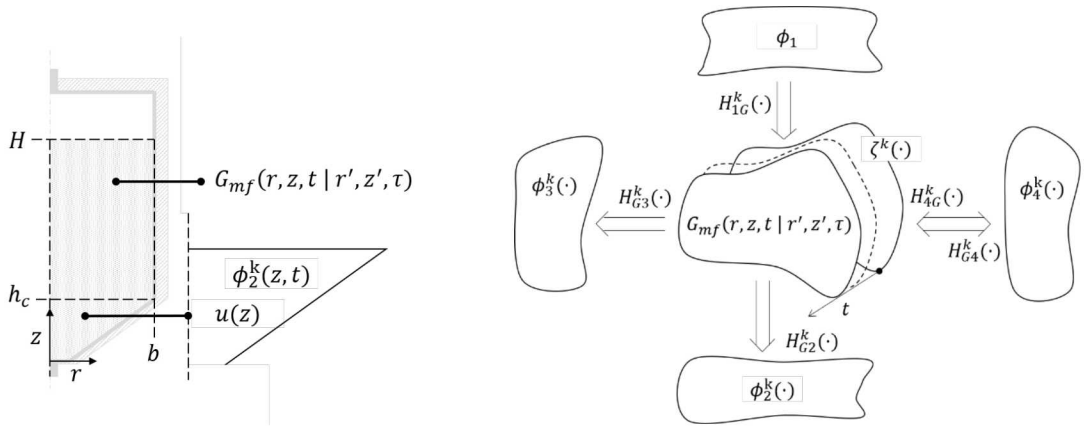

FIGURE 4. Mass flow domain separation (a) and general framework used for coupling (b)

TABLE 3. Governing equation, boundary conditions, and general solution to mass flow heat kernel boundary couplings. Initial conditions are known and arbitrary.

	Governing Eq.	z-boundaries	Solution	Notes
ϕ_1^k	–	–	cte	†
$\phi_2^k(z,t)$	$\frac{1}{\alpha}\frac{D\phi_2^k}{Dt} = \nabla^2\phi_2^k$	$\left.\frac{\partial\phi_2^k}{\partial z}\right\|_{z=0} = 0 \quad \phi_2^k\|_{z=h_c} = H_{G2}^k$	$e^{A_2^k t}\phi_2^k\|_{t_0}$	*
$\phi_3^k(z)$	–	–	$H_{G3}^k(z)$	
ϕ_4^k	–	–	T_∞	**

† 'cte' refers to a constant condition over time-step, k.

* A_2^k is the 1-D state matrix derived from a spatial discretization of the domain, updated at every time-step, k.

** Homogeneous simplification from Jaeger boundary condition shown in **FIGURE 2**.

RESULTS AND DISCUSSION

Here, we first present a verification for the heat kernel modeling approach in **FIGURE 5** by comparing the transient outlet temperature to a set of funnel flow experiments and a CFD mass flow simulation. The experiments were performed at Sandia National Laboratories in Albuquerque, NM and follow procedure published in [20]. The CFD baseline model uses a level-set approach and has also been covered in [16] and [20]. From this verification, we identify sufficient trust in the heat kernel modeling approach to provide a direct comparison of a funnel flow and mass flow system in **FIGURE 6**. Critical parameters that have physical relevance are provided in **TABLE 4** for all testing/simulation results.

The experimental verification for the level set system places particular influence on the hold time, which is the time that the particles are held stagnant (cooling) before discharge is initiated. We can see in **FIGURE 5(a)** that the cooling time has a significant impact on the outlet temperature in the lead-in period and initial temperature droop, but has a diminishing effect as time marches on. These inter-cycle periods of cooling are particularly cumbersome in the modeling process and will be a major point of focus for future efforts that adapt this modeling approach to long-term cycling applications. We would also like to point out that the heat kernel model tends to underestimate particle temperatures. It is suspected that one reason for this is that the wall boundaries are assumed to hold no thermal charge; a simplification from the Jaeger boundary condition as noted in **TABLE 2**.

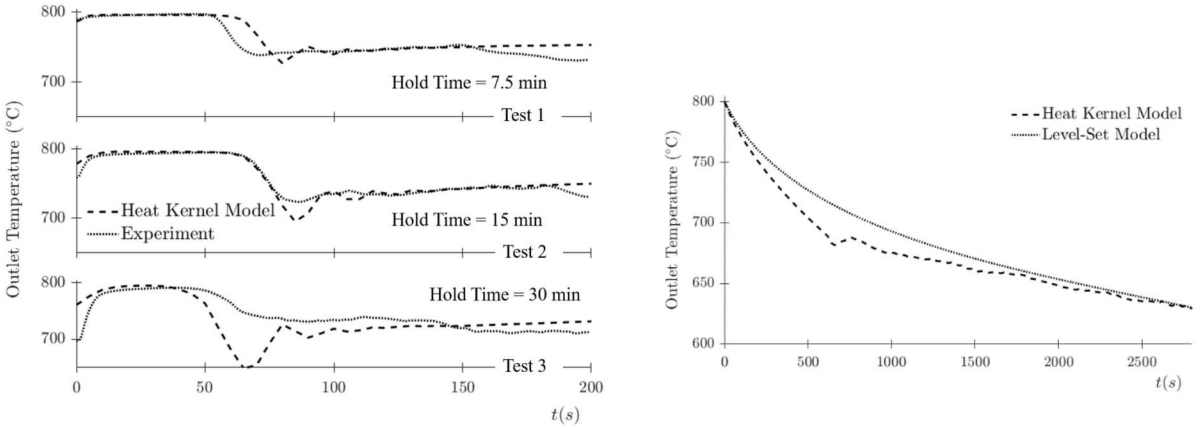

(a) (b)

FIGURE 5. Experimental verification for a funnel flow system under the three sets of conditions listed in **TABLE 3** and (b) a baseline CFD model verification for a mass flow system

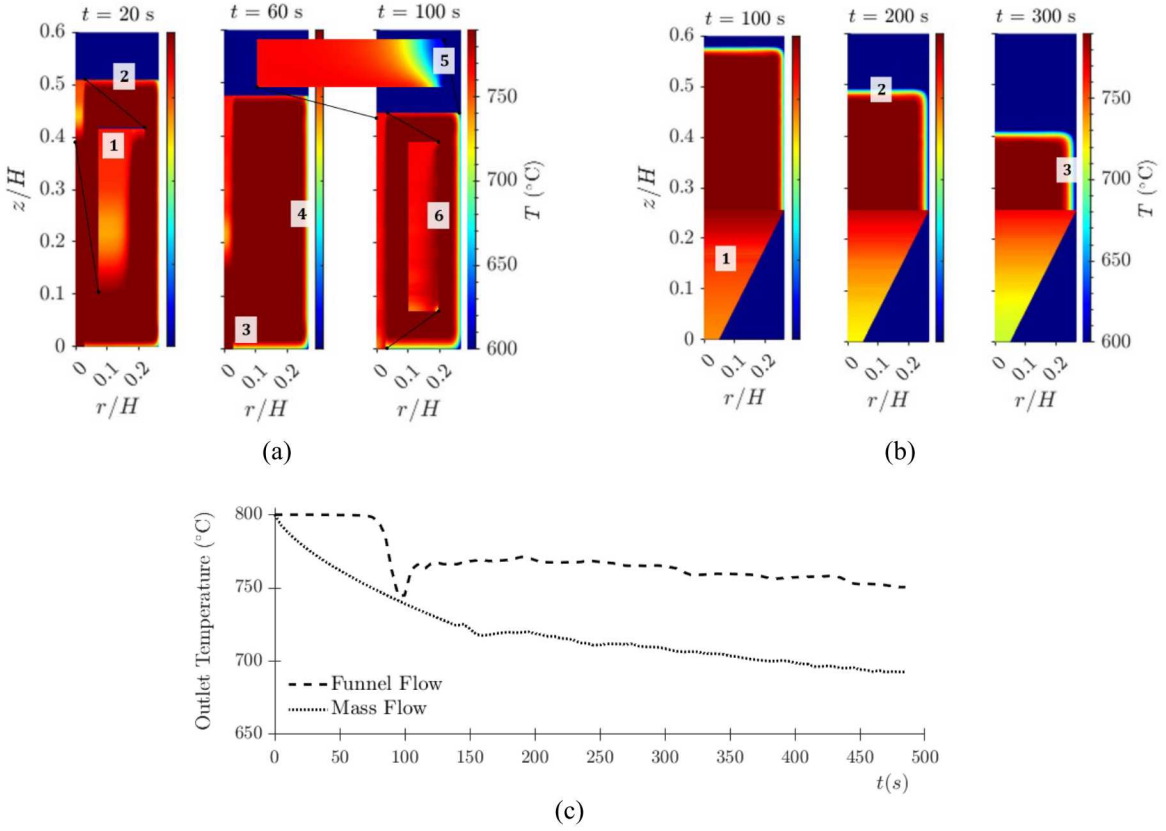

(a) (b)

(c)

FIGURE 6. Contour plots with dominant heat modes numbered for a funnel flow system (a) and mass flow system (b). The associated outlet temperatures for the same systems are plotted in (c)

TABLE 4. Select simulation and test parameters

	Hold Time (s)	**Wall Overall Heat Transfer Coefficient** $U_w\ (W/m^2K)$	**Base Overall Heat Transfer Coefficient** $U_b\ (W/m^2K)$	**Flow Rate** (kg/s)	**Starting Mass** (kg)	**Bin Radius** (m)	**Notes**
Funnel Flow Test 1	450	23.3	17.1	0.045	28.8	0.133	†
Funnel Flow Test 2	900	23.3	17.1	0.041	28.8	0.133	†
Funnel Flow Test 3	1800	23.3	17.1	0.038	21.9	0.133	†
Mass Flow Verification	0	6.76	24.7	0.019	67.0	0.133	*
Heat Kernel Flow Comparison	0	23.3	68.1 (Mass Flow) 17.1 (Funnel Flow)	0.045	29.0	0.133	**,▲

†	**FIGURE 5(a)**. Experimental verification for a funnel flow system under the three sets of conditions
*	**FIGURE 5(b)**. Baseline CFD model verification for a mass flow system
**	**FIGURE 6**. Funnel flow and mass flow comparison for heat kernel model
▲	U_b for the mass flow regime is computed with the surface area of the full flow cone

The heat kernel model simulation results shown in **FIGURE 6** serve as the reference for the classification of the dominating heat modes in these systems, with the assumption that the transient behavior in this system is upheld under scaling and operation modifications. Beginning with the funnel flow system shown in **FIGURE 6(a)**, perhaps the mode most characteristic of funnel flow is Mode 1, which is the advection of cool top-surface particles through the center flow channel. The rate at which Mode 1 operates sets the location of the initial droop seen in **FIGURE 6(c)** at 100 s, which is the motivation for a discrete sensitivity analysis on select model parameters that will be the focus of future work. Funnel flow Modes 1-4 are more straight forward and can be classified by a standard interplay characterization between advective and diffusive properties. Funnel flow Mode 5 is particularly insightful because this is the starting point for the trajectory of the coldest particles in the bin. We have found that the rebound temperature after the initial droop for $t > 100s$ in **FIGURE 6(c)** is most sensitive to this mode. The Mass flow modes are more trivial and are generally characterized by the heat loss through the bin walls and top surface (Modes 1-3). As expected, the outlet temperature is most sensitive to these losses in the flow cone region.

CONCLUSIONS

From the discussion herein, it is evident that the thermal performance of particle storage bins is multifaceted. For their application in next generation CSP, a consideration of cyclic behavior, thermal mixing within the particle domain, and deterministic attributes should be included alongside the traditional notion of overall heat loss. We propose the following considerations for bulk particle thermal storage bin performance: 1) The geometry of the bin should be such that total heat loss to the environment is minimized, 2) the kinematic and thermal behavior should be well defined and remain within isolated operating conditions (e.g. transitions from funnel flow to mass flow are avoided) and 3) the transient thermal behavior of the bin should be controllable within identifiable limits to allow for system integration.

This work suggests that the transient thermal behavior of a funnel flow system is preferable in thermal storage applications, provided that a model sufficient for design and operation is available. The heat kernel model proposed here seems to make a good case for filling this gap, and the complexity of design and operation of a funnel flow system can be relieved with further developments. Such future developments will address the detailed cyclic behavior of thermal storage at full-scale and will introduce new opportunities for the advanced control of next generation CSP.

ACKNOWLEDGMENTS

This work is funded in part or whole by the U.S. Department of Energy Solar Energy Technologies Office under Award Number 34211.

Sandia National Laboratories is a multimission laboratory managed and operated by National Technology and Engineering Solutions of Sandia, LLC, a wholly owned subsidiary of Honeywell International, Inc., for the U.S. Department of Energy's National Nuclear Security Administration under contract DE-NA0003525.

REFERENCES

1. C. K. Ho, K. J. Albrecht, L. Yue, B. Mills, J. N. Sment, J. Christian, and M. Carlson, "Overview and Design Basis for the Gen 3 Particle Pilot Plant (G3P3)," in SolarPACES 2019 Conference Proceedings, 2019.
2. K. J. Albrecht, C. K. Ho, and M. L. Bauer, "Parametric Analysis of Particle CSP System Performance and Cost to Intrinsic Particle Properties and Operating Conditions," in Proceedings of the ASME 2019 13th International Conference on Energy Sustainability, ES 2019, Bellevue, WA, USA, 2019.
3. J. N. Sment, K. J. Albrecht, J. Christian, C. K. Ho, "Optimization of Storage Bin Geometry for High Temperature Particle-Based CSP Systems," in Proceedings of the ASME 2019 13th International Conference on Energy Sustainability, ES2019, Bellevue, WA, USA, 2019.
4. A. W. Jenike, "Gravity Flow of Bulk Solids," Bulletin No. 108, Vol. 52, No. 29. Salt Lake City, UT: Utah Engineering Experiment Station, University of Utah, 1961.
5. B. C. Burman, P. A. Cundall, and O. D. L. Strack, "A discrete numerical model for granular assemblies," *Geotechnique*, vol. 30, no. 3, pp. 331–336, 1980.
6. P. A. Langston, U. Tüzün, and D. M. Heyes, "Discrete element simulation of internal stress and flow fields in funnel flow hoppers," *Powder Technol.*, vol. 85, no. 2, pp. 153–169, 1995.
7. R. M. Nedderman and U. Tüzün, "A kinematic model for the flow of granular materials," *Powder Technol.*, vol. 22, no. 2, pp. 243–253, 1979.
8. K. F. Zhang and J. Y. Ooi, "A kinematic model for solids flow in flat-bottomed silos," *Geotechnique*, vol. 48, no. 4, pp. 545–553, 1998.
9. U. Tüzün and R. M. Nedderman, "An investigation of the flow boundary during steady-state discharge from a funnel-flow bunker," *Powder Technol.*, vol. 31, no. 1, pp. 27–43, 1982.
10. K. Grudzień and M. H. D. La Torre Gonzalez, "Detection of tracer particles in tomography images for analysis of gravitational flow in silo," *Image Process. Commun.*, vol. 18, no. 2–3, pp. 11–22, 2014.
11. W. W. Mullins, "Stochastic theory of particle flow under gravity," *J. Appl. Phys.*, vol. 43, no. 2, pp. 665–678, 1972.
12. Z. Ma, P. Davenport, and J. Martinek, "Thermal Energy Storage Using Solid Particles for Long-Duration Energy Storage," in ASME 2020 14th International Conference on Energy Sustainability. American Society of Mechanical Engineers Digital Collection, 2020.
13. C. K. Ho, "A review of high-temperature particle receivers for concentrating solar power," *Appl. Therm. Eng.*, vol. 109, pp. 958–969, 2016.
14. W. L. Vargas and J. J. McCarthy, "Heat Conduction in Granular Materials," in Materials Research Society Symposium Proceedings, vol. 47, no. 5, 2001.
15. M. L. Hunt, "Discrete element simulations for granular material flows: Effective thermal conductivity and self-diffusivity," *Int. J. Heat Mass Transfer*, vol. 40, no. 13, pp. 3059–3068, 1997.
16. J. N. Sment, K. J. Albrecht, M. J. Martinez, and C. K. Ho, "Design Considerations for a Hight-Temperature Particle Storage Bin."
17. T. Baumann and S. Zunft, "Properties of granular materials as heat transfer and storage medium in CSP application," *Sol. Energy Mater. Sol. Cells*, vol. 143, pp. 38–47, 2015.
18. G. J. Cheng, A. B. Yu, and P. Zulli, "Evaluation of effective thermal conductivity from the structure of a packed bed," *Chem. Eng. Sci.*, vol. 54, no. 19, pp. 4199–4209, 1999.
19. Z. Ma, P. Davenport, and R. Zhang, "Design analysis of a particle-based thermal energy storage system for concentrating solar power or grid energy storage," *J. Energy Storage*, vol. 29, no. February, p. 101382, 2020.
20. J. N. Sment, M. J. Martinez, K. J. Albrecht, C. K. Ho, "Testing and Simulations of Spatial and Temporal Temperature Variations in a Particle-Based Thermal Energy Storage Bin," in Proceedings of the ASME 2020 14th International Conference on Energy Sustainability, ES2020, Denver, CO, USA, 2020.
21. K. D. Cole, J. V. Beck, A. Haji-Sheikh, and B. Litkouhi, *Heat Conduction Using Green's Functions*. Taylor & Francis, 2013.
22. J. K. Eaton, "The Discrete Green's Function for Convective Heat Transfer Part 1: Definition and Physical Understanding," *J. Heat Transfer*, 2020.
23. J. K. Eaton and P. M. Milani, "The Discrete Green's Function for Convective Heat Transfer Part 2: Semi-Analytical Estimates of Boundary Layer DGF's," *J. Heat Transfer*, 2020.
24. A. Haji-Sheikh, J. V. Beck, and K. D. Cole, "Steady-state Green's function solution for moving media with axial conduction," *Int. J. Heat Mass Transf.*, vol. 53, no. 13–14, pp. 2583–2592, 2010.
25. T. W. Tu and S. Y. Lee, "Analytical Solution of Heat Conduction for Hollow Cylinders with Time-Dependent Boundary Condition and Time-Dependent Heat Transfer Coefficient," *J. Appl. Math.*, vol. 2015, 2015.
26. M. N. Özisik, *Heat conduction*. John Wiley & Sons, 1980.
27. D. W. Hahn and M. N. Özisik, *Heat conduction*. John Wiley & Sons, 2012.